# Hydrogen/Deuterium Exchange and Molecular Dynamics Analysis of Amyloid Fibrils Formed by a D69K Charge-Pair Mutant of Human Apolipoprotein C-II

Yu Mao,[†] Courtney O. Zlatic,[†] Michael D. W. Griffin,[†] Geoffrey J. Howlett,[†] Nevena Todorova,[‡] Irene Yarovsky,[‡] and Paul R. Gooley*[,†]

[†]Department of Biochemistry and Molecular Biology, Bio21 Molecular Science and Biotechnology Institute, University of Melbourne, Parkville, Victoria 3010, Australia

[‡]Health Innovations Research Institute, RMIT University, GPO Box 2476, Melbourne, Victoria 3001, Australia

Ⓢ *Supporting Information*

β-core (side view)
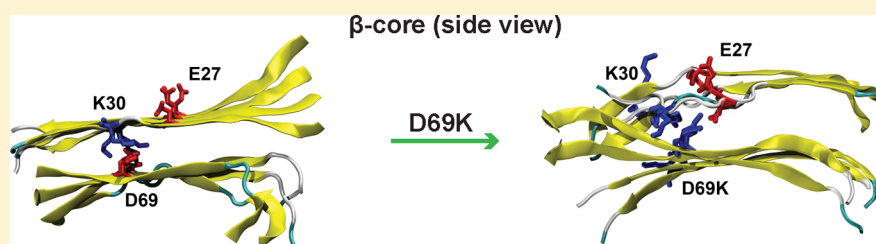
ABSTRACT: Plasma apolipoproteins form amphipathic α helices in lipid environments but in the lipid-free state show a high propensity to form β structure and self-associate into amyloid fibrils. The widespread occurrence of apolipoproteins in amyloid plaques suggests disease-related roles, specifically in atherosclerosis. To reconcile the dual abilities of apolipoproteins to form either α helices or cross-β sheet structures, we examined fibrils formed by human apolipoprotein C-II (apoC-II). A structural model for apoC-II fibrils shows a cross-β core with parallel β strands, including a buried K30-D69 charge pair. We investigated the effect of abolishing this charge pair in mutant D69K apoC-II. Fluorescence studies indicated more rapid fibril formation and less solvent accessibility of tryptophan (W26) in D69K apoC-II fibrils than in wild-type (WT) fibrils. X-ray diffraction data of aligned D69K apoC-II fibrils yielded a typical cross-β structure with increased β sheet spacing compared to that of WT fibrils. Hydrogen/deuterium (H/D) exchange patterns were similar for D69K apoC-II fibrils compared to WT fibrils, albeit with an overall reduction in the level of slow H/D exchange, particularly around residues 29−32. Molecular dynamics simulations indicated reduced β strand content for a model D69K apoC-II tetramer compared to the WT tetramer and confirmed an expansion of the cross-β spacing that contributed to the formation of a stable charge pair between K69 and E27. The results highlight the importance of charge-pair interactions within the apoC-II fibril core, which together with numerous salt bridges in the flexible connecting loop play a major role in the ability of lipid-free apoC-II to form stable cross-β fibrils.

Amyloid fibrils accumulate within plaques in a number of common and debilitating diseases, including Alzheimer's and Parkinson's disease and type II diabetes.[1] Plasma apolipoproteins are prevalent within the list of proteins that have been identified within amyloid deposits *in vivo*. The list includes apolipoprotein (apo) A-I,[2] apoA-II,[3] apoA-IV,[4] apoC-II,[5] and apoE[6] as well as the apolipoprotein-related proteins α-synuclein and serum amyloid A.[1] Histological studies demonstrate the accumulation of several plasma apolipoproteins within atherosclerotic plaques, raising the possibility of a causative role in the development of atherosclerosis.[5,7] Considerable attention has focused on the universal presence of apoE in amyloid plaques in view of the strong genetic linkage with specific isoforms of apoE and Alzheimer's disease.[8] *In vitro* studies reveal several lipid-free apolipoproteins readily form fibrils with all the properties of amyloid fibrils, including a cross-β structure, red−green birefringence in the presence of Congo Red, and the ability to bind the dye thioflavin T.[9] The widespread occurrence of apolipoproteins

within amyloid deposits and the general propensity of apolipoproteins to form amyloid fibrils *in vitro* suggest common structural features that predispose them to amyloid fibril formation.

Amino acid sequence comparisons within the apolipoprotein superfamily reveal a high level of conservation derived from duplications of an ancestral repeat.[10] This repeat unit coincides with shared structural features, specifically a high proportion of class A amphipathic α-helical domains that mediate the binding to lipoprotein surfaces. Class A amphipathic α helices are characterized by lysine residues at the junction of the hydrophilic and hydrophobic surfaces of the helix and negatively charged residues positioned centrally in the polar surface. This distribution of charged residues, especially from the lysine residues, is

considered to provide stabilizing interactions with the phosphate and choline moieties of the phospholipid headgroups that anchor the protein to the phospholipid surface.[11] It has been proposed that in the absence of lipid surfaces apolipoproteins have limited conformational stability leading to misfolding and amyloid formation.[12] It is of interest to contrast the ability of the apolipoprotein superfamily to form class A amphipathic helices with the high propensity of this class of proteins to form amyloid fibrils. Amphipathic helices contain hydrophilic residues distributed on the polar face and thus separated by three or four residues within the sequence, consistent with a rise of approximately 3.6 amino acids per turn of the helix. This raises the question of how such structures are compatible with the formation of a cross-β structure where every second amino acid residue is located within the hydrophobic core of the amyloid fibril.

Extensive structural studies of amyloid fibrils formed by lipid-free human apoC-II led to the development of a structural model[13] that provides some insight into this question. The model consists of a three-layered β-strand−loop−β-strand structure with the two β strands, encompassing residues 20−36 and 58−74 of apoC-II, in parallel register within monomer units and parallel within the cross-β sheets. Molecular dynamics (MD) simulations show that loop flexibility allows the charge clusters to rearrange to minimize repulsive interactions inherent in parallel-in-register models. An integral part of the model is the existence of a buried charge pair involving K30 and D69 within the cross-β core of the fibrils. These residues are present in a lipid binding region[14] and a highly conserved α-helical lipoprotein lipase-activating region, respectively.[15] The formation of the buried K30-D69 charge pair within apoC-II fibrils reconciles the dual abilities of apoC-II to form class A amphipathic helices and cross-β structure in lipid and lipid-free environments, respectively. To explore the role of the K30-D69 charge pair, we have previously studied the fibril forming ability of a D69K charge-pair mutant of apoC-II.[16] This study describes the effects of this mutation on the structural properties of apoC-II amyloid fibrils.

■ MATERIALS AND METHODS

Preparation of ApoC-II. Expression and purification of wild-type (WT) apoC-II and D69K apoC-II were performed as described previously.[16] [15]N enrichment of WT and D69K apoC-II was achieved using a modification of published methods.[17,18] Purified apoC-II stock solutions (30−45 mg/mL) were stored at −20 °C in 5 M guanidine hydrochloride (GuHCl) and 10 mM Tris-HCl (pH 8.0).

Fibril Formation. Fibril formation was performed by dilution of the protein stocks (30−40 mg/mL) to either 0.3 or 1 mg/mL in refolding buffer [100 mM sodium phosphate buffer and 0.1% sodium azide (pH 7.4)], followed by incubation under quiescent conditions at room temperature (22 °C) for 5 days.

Fluorescence Spectroscopy. Fluorescence measurements for apoC-II samples were conducted using a Cary Varian Eclipse fluorescence spectrophotometer (Agilent Technologies Inc.) at 20 °C. Tryptophan emission spectra were collected over the wavelength range of 300−450 nm with an excitation wavelength of 295 nm. Fluorescence quenching experiments were performed on apoC-II samples using acrylamide as an external quencher at concentrations ranging from 0 to 0.3 M. Serial additions of acrylamide (2 μL of 2 M) were added and mixed thoroughly with the samples. The excitation wavelength was set at 295 nm, while the emission wavelengths for the fibril samples and freshly prepared samples were set to 344 and 357 nm, respectively.

Stern−Volmer plots were constructed, and the effective quenching constants (K_D) were determined by linear regression analysis based on the Stern−Volmer equation:

$$\frac{F_0}{F} = 1 + K_D[Q] \tag{1}$$

where F_0 and F are the fluorescence intensities of the unquenched and quenched fluorophore, respectively, and $[Q]$ is the molar concentration of the quencher.

Hydrogen/Deuterium (H/D) Exchange Measurements by NMR Spectroscopy. Hydrogen/deuterium (H/D) exchange methods were used to map the β-core structure of amyloid fibrils formed by ^{15}N-labeled apoC-II variants. The extent of incorporation of deuterium into fibril samples was monitored using [1]H−[15]N heteronuclear single-quantum coherence (HSQC) spectra obtained at a series of time points following the initiation of hydrogen exchange with deuterium. To achieve this, a quenched H/D exchange approach[19] was applied to the fibril samples. The experimental procedure consisted of four steps (fibril formation, H/D exchange, quenching, and dissolution), followed by NMR analysis.

Fibril formation of ^{15}N-labeled apoC-II samples was performed under standard conditions to a final concentration of 1 mg/mL. Mature fibrils were collected by centrifugation at 100000 rpm for 30 min (MLA 130 rotor, OptimaMax centrifuge). One pellet fraction obtained from a sample aliquot of 500 μL was kept separate for acquiring a [1]H−^{15}N HSQC reference spectrum of the fully protonated sample. This pellet fraction was immediately snap-frozen in liquid nitrogen and stored at −20 °C. To initiate deuterium incorporation, the remainder of the pellet fractions were resuspended in 2.5 mM Tris-HCl buffer and 100% D₂O (pH 7.4) (uncorrected glass electrode reading) and incubated at 22 °C. At selected time points (0.5, 24, 72, and 168 h), fibril samples were collected by centrifugation at 100000 rpm for 30 min and the resulting pellet fractions were snap-frozen in liquid nitrogen and stored at −20 °C. The frozen pellets were solubilized for 10 min in a solution containing 95% (v/v) d_6-dimethyl sulfoxide (DMSO), 4.5% D₂O, and 0.5% d_2-dichloroacetic acid (d_2-DCA) (pH 4.3) (uncorrected glass electrode reading) and then transferred to NMR tubes immediately for spectral measurement. Under these conditions, exchange is quenched but not completely stopped,[20,21] and therefore, to account for differential exchange of individual residues, we prepared a reference sample of fully protonated fibrils that were dissolved in the d_6-DMSO/D₂O/d_2-DCA buffer for NMR data acquisition under the same conditions. Measurements were performed on a Bruker AVANCE III HD 700 MHz NMR spectrometer equipped with a triple-resonance cryoprobe. Two-dimensional [1]H−^{15}N HSQC spectra for each H/D exchange sample and reference samples were obtained at 25 °C using a spectral width of 6000 Hz and 2048 complex points in the ^{1}H dimension, and a spectral width of 1024 Hz in the ^{15}N dimension with 256 t_1 increments. Data were processed using NMRPipe[22] and analyzed in NMRView,[23] as previously reported.[19]

X-ray Diffraction. ApoC-II fibril samples at 0.3 mg/mL were pelleted by centrifugation at 100000 rpm for 30 min (TLA-100 rotor, OptimaMax centrifuge), followed by resuspension in distilled water. This process was repeated three times to remove buffer salts. The final resulting fibril pellet was then resuspended in a small volume of distilled water to a final concentration of approximately 10 mg/mL. Fibrils were aligned using a modification of the stretch frame method as previously described.[24] X-ray diffraction images were acquired at the Australian
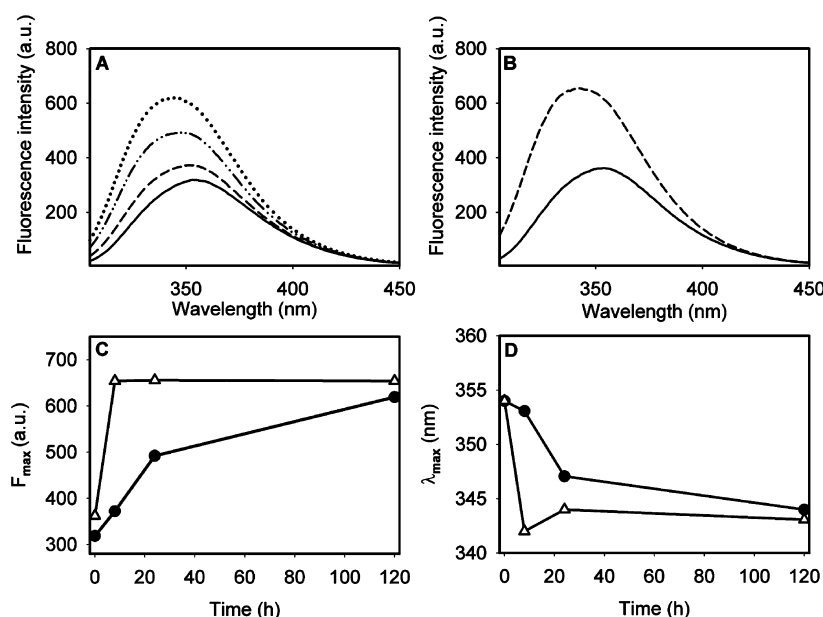
Figure 1. Tryptophan fluorescence emission spectra of apoC-II samples during fibril incubation. ApoC-II samples (0.3 mg/mL) were incubated in refolding buffer at 22 °C. The excitation wavelength was 295 nm. Emission spectra of (A) WT apoC-II and (B) D69K apoC-II were collected immediately after the initiation of refolding (—) and following incubation for 8 h (– – –), 24 h (–··–), and 120 h (···). In panel B, the 24 and 120 h spectra overlapped with the 8 h spectra and were omitted from the figure for the sake of clarity. (C and D) Maximal emission fluorescence intensity (F_{max}) and wavelength (λ_{max}) corresponding to the emission maximum for WT (●) and D69K (△) vs incubation time.

Synchrotron MX2 beamline (λ = 0.9184 Å). The sample-to-detector distance was 140 mm, and the exposure time was 5 s. A processed image was obtained by using a raw diffraction image and subtracting an image of background air scattering, which was obtained under identical conditions with no sample in the beam. The processed diffraction images were then analyzed using the software package CLEARER.[25]

Molecular Dynamics Simulations. A stable full-length WT apoC-II fibril tetramer, identified in our previous work,[13] was used as a starting structure for molecular dynamics (MD) simulations of the mutated D69K aggregate. Explicit solvent MD simulations were conducted on the D69K apoC-II mutant tetramer using the GROMACS 4.6.5 (www.gromacs.org) simulations package. The interatomic interactions were treated using the GROMOS force field parameter set 43A1 and the SPC water model. Electrostatic interactions were evaluated using the particle-mesh Ewald (PME) method; van der Waals interactions were truncated at 10 Å. The D69K apoC-II tetramer model was enclosed in a periodic cubic box sufficiently large to avoid significant cross-cell interactions with a minimal distance between the solute and the edges of the box of 12 Å. The simulation box was solvated with 56073 SPC water molecules, corresponding to a water density of ~1.0 g/cm³. The apoC-II tetramer charge of −8 was compensated by adding eight Na⁺ counterions to ensure a neutral simulation cell. The MD simulations were conducted under constant particle number, pressure, and temperature (NPT) conditions with the target temperature maintained via the velocity rescaling method,[26] where the solvent and protein were coupled separately to a temperature bath at 300 K with a temperature coupling constant of 0.1 ps. Pressure coupling was performed using the Parrinello−Rahman scheme.[27] A constant pressure of 1 bar and a pressure coupling constant of 1.0 ps were applied uniformly for the system. Bond lengths were constrained using the LINCS algorithm.[28] An integration time step of 2 fs was used. The whole system was initially energy minimized to remove steric clashes using the steepest descent approach.

To allow the solvent to relax around the protein, MD equilibration was performed for 100 ps with the protein fibril restrained. Unrestrained simulation was performed for 160 ns, in which reaching the equilibrium was monitored by following the evolution of the total energy and root-mean-square deviation, which plateaued after simulation for 100 ns, and the last 60 ns was used for data analysis. Visualization of system geometries and interactions and evaluation of protein secondary structure and ion-pair (salt bridge) formation were performed using the visual molecular dynamics (VMD) environment.[29] A salt bridge was considered formed if the distance between any oxygen atoms of an acidic residue side chain and the nitrogen atoms of a basic residue side chain was less than 3.2 Å. The intersheet and interstrand spacing were determined from the middle two strands of the tetramer by taking the average of the backbone center-of-mass distance separations of opposing (facing) residues within the two β strands (encompassing residues 20−36 and 58−74). Root-mean-square fluctuation (rmsf) analysis was employed to measure the deviation (dynamics) of W26 during equilibrium. To quantify the hydration level of the β core, the number of water molecules present in the first hydration shell (within 3 Å) of the β-sheet strands was determined (averaged over the last 1 ns of simulation).

Analysis of Fibril Stability. Fibril stabilities were examined using a GuHCl denaturation assay.[30] Preformed WT and D69K apoC-II fibrils were added at a final concentration of 0.3 mg/mL to specified final concentrations of GuHCl. Samples were vortexed and incubated at room temperature for 24 h prior to centrifugation at 100000 rpm (436000g) for 30 min at 20 °C in an OptimaMax centrifuge using a TLA-100 rotor (Beckman Coulter Instruments, Inc., Fullerton, CA). The supernatants were immediately removed, and the protein concentration was determined by optical absorbance measurements at 280 nm using a DU-800 UV/vis spectrophotometer (Beckman Coulter). The proportion of apoC-II in the supernatant was determined from their optical absorbances relative to uncentifuged samples

solubilized in the presence of 6 M GuHCl. The GuHCl concentrations at half-maximal dissociation ($c_{1/2}$) for both WT and D69K were derived from fits to a four-parameter sigmoid function.

RESULTS

Time-Dependent Change in Tryptophan Fluorescence during Fibril Formation. We monitored the change in the fluorescence on fibril formation of the single tryptophan (W26) in WT apoC-II and D69K apoC-II using fluorescence emission measurements (Figure 1). W26 in both WT apoC-II and D69K apoC-II showed an increase in its maximal fluorescence intensity during the fibril incubation period. In the freshly refolded state, the maximal fluorescence intensities of WT apoC-II and D69K apoC-II were approximately 320 and 360 au, respectively. These maxima occurred at an emission wavelength of 354 nm. Over the incubation time, D69K apoC-II showed a more rapid increase in the maximal fluorescence intensity compared to that of WT apoC-II, reaching a plateau value within 8 h, while the maximal fluorescence intensity for WT apoC-II changed slowly over a period of 120 h. The observed rates of changes in maximal fluorescence intensities are attributed to more rapid fibril formation by D69K apoC-II, consistent with previous studies.[16] The wavelength corresponding to the emission spectral peak for both WT apoC-II and D69K apoC-II samples showed a blue shift of approximately 10 nm during the incubation period, which can be attributed to the transition of W26 to a more hydrophobic environment.

Acrylamide Quenching Analysis. The accessibility of W26 in WT apoC-II and D69K apoC-II to solvent was determined using an acrylamide fluorescence quenching approach and evaluated by Stern−Volmer plots (Figure 2). Quenching constants for
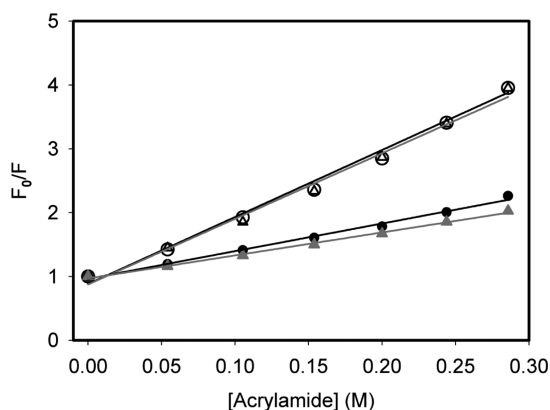
Figure 2. Stern−Volmer plots for acrylamide quenching of the tryptophan fluorescence in apoC-II samples: freshly prepared WT apoC-II (○), freshly prepared D69K apoC-II (△), WT apoC-II fibrils (●), and D69K apoC-II fibrils (gray triangles). The best-fit lines drawn through the data based on eq 1.

freshly prepared samples of WT apoC-II and D69K apoC-II were at least 2.5-fold greater than for fibril samples formed by WT apoC-II and D69K apoC-II (Table 1), indicating that W26 in the freshly prepared samples is more exposed to the solvent than W26 in the fibril samples. An additional observation is the quenching constant for fibrils formed by D69K apoC-II is approximately 15% lower than for WT apoC-II fibrils, indicating less accessibility to the quenching agent.

H/D Exchange Studies. H/D exchange experiments[31] were used to measure the exchangeability of amide protons of specific

Table 1. Fluorescence Quenching of ApoC-II Variant Samples

|	K_D (M^{-1})[c]
WT monomer[a]	10.5 ± 0.1
D69K monomer[a]	10.3 ± 0.1
WT fibrils	4.3 ± 0.04
D69K fibrils[b]	3.6 ± 0.03

[a]Samples (0.05 mg/mL) were freshly refolded in refolding buffer. [b]Samples (0.3 mg/mL) were refolded in refolding buffer and incubated at 22 °C for 5 days. [c]The quenching constants, K_D, are the slopes of the Stern−Volmer plots in Figure 2.
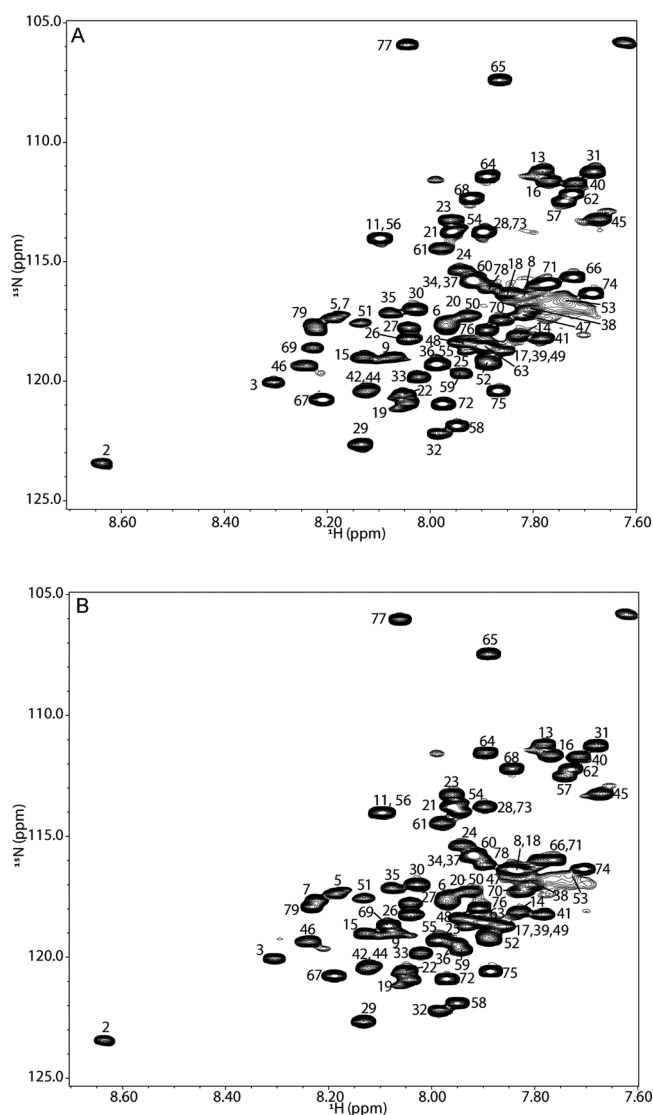
Figure 3. 2D $^1H-^{15}N$ HSQC spectra for fully protonated [^{15}N]apoC-II amyloid fibrils freshly dissolved and dissociated in 95% d_6-DMSO, 5% D_2O, and 0.2% d_2-DCA: (A) WT apoC-II and (B) apoC-II D69K. Residue specific assignments are indicated.[31]
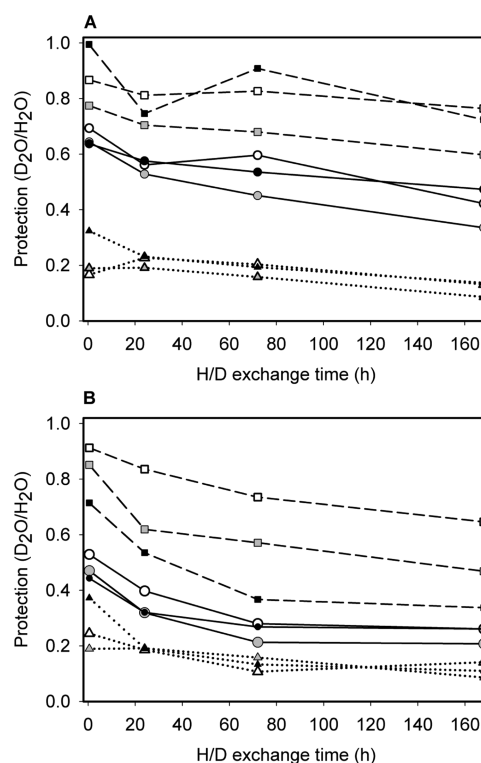
amino acid residues in fibrils formed by [^{15}N]WT apoC-II and [^{15}N]apoC-II D69K. Two-dimensional (2D) $^1H-^{15}N$ HSQC NMR spectra for fibril samples exposed to D_2O over 0.5, 24, 72, and 168 h as well as protonated reference samples were collected following solubilization and dissociation of the fibril in d_6-DMSO/D_2O/d_2-DCA buffer. The spectra of samples of protonated [^{15}N]WT apoC-II showed ^{15}NH chemical shifts (Figure 3A) that were similar to the sequential resonance
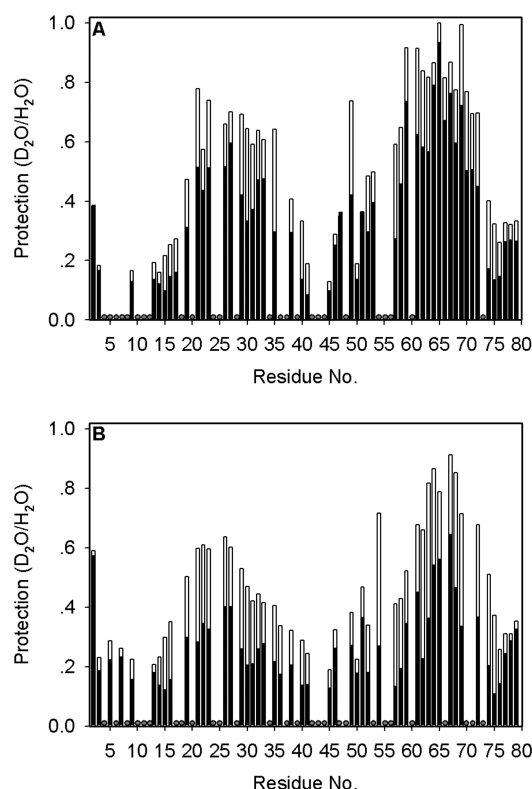
Figure 4. Residue specific protection of the backbone amides in fibrils formed by (A) WT apoC-II and (B) D69K apoC-II. The protection ratios are expressed as peak intensities for fibril samples subjected to H/D exchange relative to fully protonated fibril samples for 0.5 h (white bars) and 168 h (black bars). Residues indicated by gray circles are proline residues or insufficiently resolved in the 2D ^{1}H$-^{15}$N HSQC spectra to unambiguously measure intensity changes (Figure 3).

Figure 5. Exchange kinetics for well-resolved peaks identified in 2D ^{1}H$-^{15}$N HSQC spectra for amyloid fibrils formed by (A) [^{15}N]WT apoC-II and (B) [^{15}N]D69K apoC-II. Representative data for residues located in unprotected regions (⋯): M9 (△), Y41 (gray triangles), and L75 (▲). Representative data for residues located in the first β strand (—): A29 (○), K30 (gray circles), and A32 (●). Representative data for residues located in the second β strand (- - -): F67 (□), T68 (gray squares), and D69 (■).

assignments of [^{13}C,^{15}N]WT apoC-II reported previously.[31] Spectra of D69K apoC-II (Figure 3B) showed peaks assigned to residues 68−71 were significantly shifted while the positions of all other peaks were similar to those of the WT apoC-II spectra. Of a predicted number of 74 peaks for WT apoC-II and D69K apoC-II spectra, 52 and 50 ^{15}NH resonance peaks, respectively, were sufficiently well-resolved for their peak intensities to be unambiguously measured.

The degree of H/D exchange for each residue was evaluated by the ratio of the corresponding peak intensity between the exchanged and protonated sample spectra prepared and acquired under the same conditions.[21] The results in Figure 4 show the protection ratio of the amide protons of individual amino acid residues in WT apoC-II and D69K apoC-II fibrils subjected to H/D exchange over periods of 0.5 and 168 h. Samples obtained immediately after D$_2$O treatment (0.5 h) yielded a range of protection ratios indicating regions within the fibrils with both high and low rates of H/D exchange. Several residues yielded low protection ratios of approximately 0.2, which were similar to the values from control experiments using fibrils formed in the presence of D$_2$O (Figure S3). In contrast, residues 19−37 and 57−74 within the cross-β sheet regions of the fibrils[13] showed much higher levels of protection. The overall levels of protection within the core of the cross-β sheet regions were higher for WT apoC-II than for D69K apoC-II fibrils, indicating a destabilization of the fibrils that can be attributed to the D69K mutation. Further reductions in the protection ratios were observed following incubation of the samples in D$_2$O for longer periods.

The peaks with high protection ratios at 0.5 h remained prominent after incubation for 168 h. For both WT apoC-II and D69K apoC-II fibrils, amide protons of residues 19−35 and 57−72 remained as the most protected regions, indicating the overall fibril structure of D69K apoC-II fibrils is very similar to that of WT apoC-II fibrils.

The exchange kinetics of representative residues with well-resolved spectral peaks are presented in Figure 5. Residues M9, Y41, and L75 in both WT apoC-II and D69K apoC-II fibrils show low protection ratios at each time point, indicating rapid H/D exchange rates, consistent with their location within flexible regions of the fibrils. For WT apoC-II fibrils, representative residues A29, K30, and A32 within the first β strand and residues F67, T68, and D69 within the second β strand undergo a relatively slow decay in protection ratios, indicating relatively stable secondary structure. By comparison, these same β-strand residues within D69K apoC-II fibrils show lower initial protection ratios and a more rapid decay consistent with a destabilization of the fibrils caused by the D69K mutation. This conclusion is supported by kinetic data obtained for a wider range of residues located within the fibril core (Figures S1 and S2).

X-ray Diffraction Analysis. The presence of cross-β structure packing in apoC-II amyloid fibrils was assessed using X-ray fiber diffraction (XRD). The XRD images (Figure 6) showed a classical cross-β diffraction pattern with dominating reflections on the meridional and equatorial axes for both fibrils formed by WT and D69K apoC-II. The strong sharp meridional reflection at approximately 4.6 Å corresponds to the distance between the
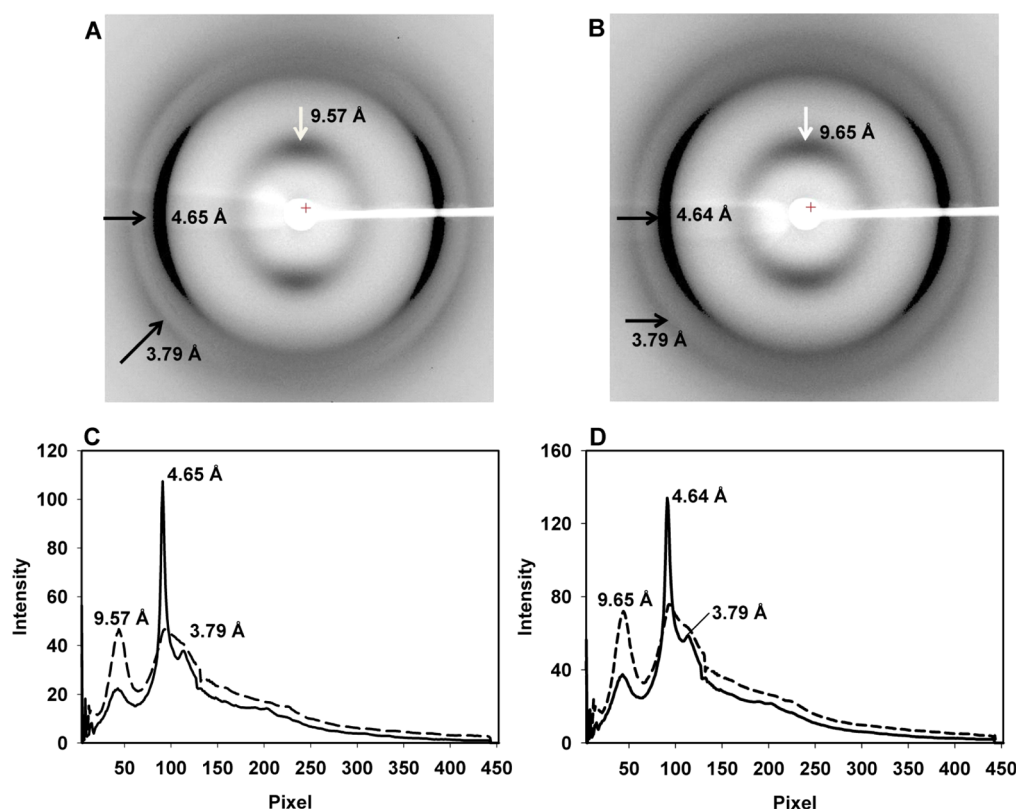
Figure 6. X-ray fibril diffraction images of (A) WT apoC-II and (B) D69K apoC-II fibrils. Equatorial reflections on the vertical axis are indicated with a white arrow; meridional reflections are indicated on the horizontal axis with black arrows. (C and D) Radial profiles for panels A and B, respectively. The spacings of equatorial (– – –) and meridional (—) reflections are indicated by the major peaks.

β strands along the fibril axis. A more diffuse equatorial spacing around 10 Å corresponds to the intersheet spacing of the fibrils. A much weaker, meridional reflection with a spacing of 3.79 Å was also observed for fibrils formed by WT apoC-II and D69K apoC-II as a shoulder on the outer edge of a diffuse scattering ring. This indicates further order within the structure of the fibril axis, which has also been reported in other amyloid systems.[32] The results in Table 2 show that the meridional spacings for D69K apoC-II fibrils compared to WT apoC-II are similar ($p > 0.05$) whereas the equatorial spacings differ ($p < 0.001$). This difference in equatorial spacing is attributed to an increased distance between the β sheets within D69K apoC-II fibrils.

Molecular Dynamics (MD) Simulations of the D69K ApoC-II Tetramer Mutant. Explicit solvent MD simulations were performed on the D69K apoC-II tetramer, and the data collected were compared to those of the previously modeled WT apoC-II fibrils.[13] Cartoon representations of the WT and the equilibrium structure of the mutated D69K apoC-II tetramer are shown in panels A and D of Figure 7. The simulations of the D69K mutant showed the tetramer generally retained the typical "letter-G-like" β-strand–loop–β-strand structure of WT apoC-II fibrils, in spite of a minor distortion of β-sheet structuring in the outer ($\beta1$ sheet) region. The disruption of the β-strand content occurred because of the same-charge repulsions between K30 and K69, which caused some swelling in this region (Figure 7E,F) and an increase in the β-sheet spacing to 9.64 ± 0.54 Å in D69K, compared to that in the WT fibril model (9.08 ± 0.4 Å). This restructuring caused the nearby glutamate (E27) to enter deeper into the β core to balance out the highly cationic environment. The increased mobility within this region also allowed an increased level of water (~7%) in the area compared to that in the WT fibril.

Table 2. Analysis of X-ray Diffraction and MD Simulation Data for WT and D69K ApoC-II Fibrils

|	meridional spacing[a] (Å)		equatorial spacing[a] (Å)
WT	3.79 ± 0.01	4.65 ± 0.01	9.57 ± 0.02
D69K	3.79 ± 0.01	4.64 ± 0.01	9.65 ± 0.02
	$p = 0.83^b$	$p = 0.19^b$	$p < 0.001^b$
MD-simulated structure	β-strand spacing (Å)		β-sheet spacing (Å)
WT	5.11 ± 0.53		9.08 ± 0.40
D69K	5.24 ± 0.31		9.64 ± 0.54

[a]The spacing data were obtained from the major peaks in the radial profiles, which were derived using CLEARER to analyze the images from different sections of the aligned sample. [b]p values refer to the comparison of spacings for WT and D69K fibrils with $n = 4$ and $n = 6$, respectively.

Nevertheless, the average distance between the β strands of D69K (5.24 ± 0.31 Å) was similar to that of the WT fibrils (5.11 ± 0.53 Å), which demonstrates the overall retention of cross-β structure packing in solution. Importantly, the physical model dimensions obtained from the MD simulations are in line with the meridional and equatorial spacing determined by our X-ray diffraction studies (Table 2).

To examine further the structural features and stability of the mutated D69K apoC-II oligomer, the β-strand propensity was calculated for each residue, defined as the amount of time each residue spends in a β-sheet backbone conformation during the final 60 ns of simulation (Figure 8). The percentages were taken as an average over the four monomers, where the standard deviations relate to the difference in β content for each residue in different monomers. The data show that the β-stranded regions
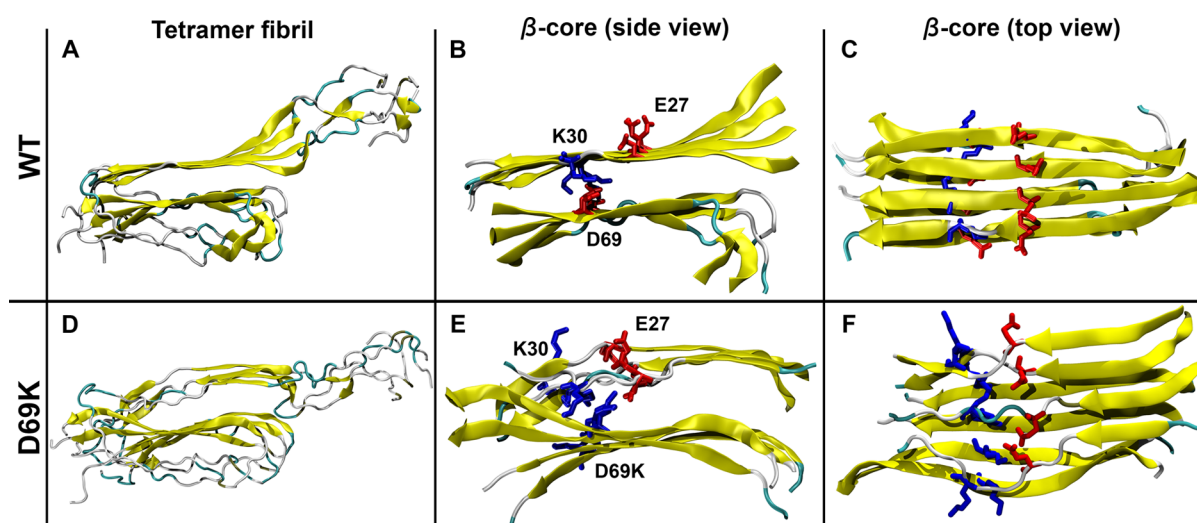
Figure 7. Molecular dynamics simulations of D69K fibrils. MD snapshots of the equilibrium conformations are colored on the basis of secondary structure elements (yellow for β strand, white for coil, and cyan for turn) of the (A) WT and (D) D69K tetramer. The central β-core structure and arrangement of ionic residues K30 and E27 (shown as licorice) near residue 69 are shown from side and top views of the WT (B and C) and D69K (E and F) fibrils, respectively.
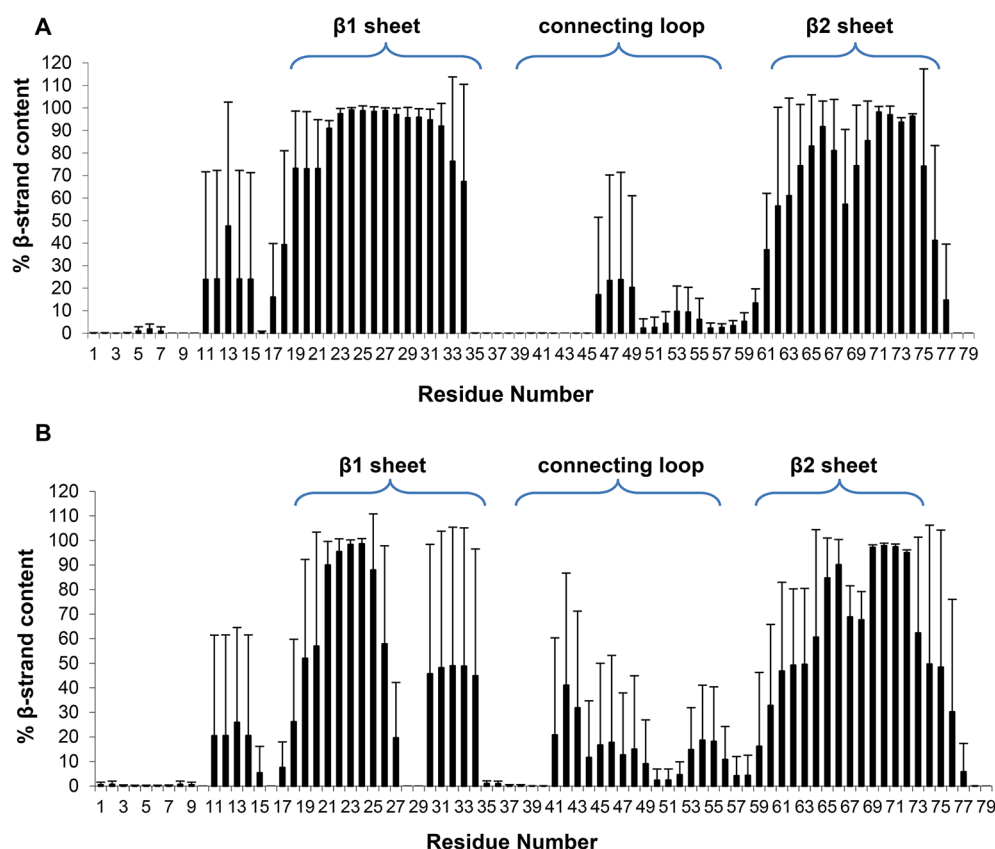
Figure 8. Percentage of time each residue spends in the β-strand conformation at equilibrium from the (A) WT[13] and (B) D69K tetramer simulations. The two β-strand regions (20−36 and 58−74) and connecting loop identified previously in the WT apoC-II fibril are labeled with braces for reference.

between residues 20−34 (β1 sheet) and 59−75 (β2 sheet) retain their β-sheet structure for the entire trajectory of each tetramer (Figure 8), although with a probability lower than that of our WT model.[13] In accordance with the H/D exchange studies, some subtle differences between WT and D69K apoC-II fibrillar structure were observed in MD simulations. A decrease in β-strand content can be seen in the outer β1 sheet between

residues A29 and Q34, which is due to the like-charge repulsion induced by K30 and K69, as highlighted in Figures 7 and 8. The significant decrease in β-structure content ($\sim$19%) compared to that of the WT fibrils suggests an increase in structural flexibility and solvent exposure of the D69K fibril, confirmed by the decreased protection ratios seen for D69K compared to WT fibrils in the H/D exchange experiment.
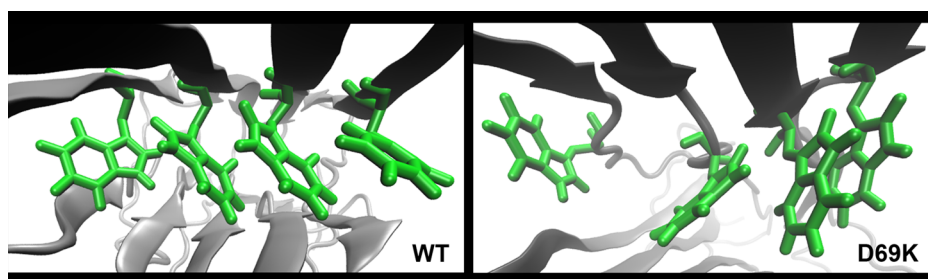
Figure 9. Equilibrium MD snapshots of the aromatic ring structuring of neighboring W26 in vicinal chains (green). The WT fibril exhibited in-register π-stacking (left), while the D69K fibril features less ordered aromatic arrangements (right).

The decreased stability in the core region associated with the formation of the new ionic pair between K69 and E27 in the mutant and the K69 repulsion from K30 causes perturbations in the positioning of the neighboring W26 residues. Specifically, in the WT fibril, W26 residues are seen to form in-register π-stacks. In contrast, residues within the D69K fibril are less ordered, forming a variety of relative orientation angles between the aromatic rings in the vicinal chains (Figure 9). This coincides with the higher mobility in the mutant and the higher level of water near the aromatic rings. This behavior is seen from rmsf analysis, which showed an ~27% increase in the dynamics of W26 in D69K compared to those of the WT fibril, as calculated over the last 10 ns of simulations.

The positional distribution of charged residues in the fibril model demonstrates that ion pairs play a major role in the formation and stability of the fibril structure. The presence of multiple salt bridges in D69K apoC-II fibrils that are also present in WT fibrils shows that charged residues contribute to the stabilization of aggregate structure (Figure 10). Specifically, for both WT and D69K apoC-II fibrils, the ion pairs within the β core (K19:E20) and connecting loop (E47:K48, E47:R50, and D51:K55) exhibited lifetimes (>20% occurrence) longer than the lifetimes of those near the C-terminal loop region (K76:E79, K39:E78, and K39:E79), which were more transient in nature (<10% occurrence). The simulations showed that for D69K fibrils the same-charge repulsion between the neighboring K30 and K69 residues in WT fibrils was compensated by the electrostatic attraction between K69 and the nearby cationic E27 with the formation of a stable (~50%) E27-K69 salt bridge (Figure 10).

Analysis of Fibril Stabilities. The results of the H/D exchange experiments (Figures 4 and 5) indicated the D69K mutation caused a decrease in the level of exchange protection in the amyloid core region that can be attributed to a destabilization of the fibrils. This assertion was tested using GuHCl denaturation assays.[30] The results in Figure 11 show distinct denaturation profiles for WT and D69K apoC-II fibrils with $c_{1/2}$ values of 1.5 and 1.1 M GuHCl, respectively. This difference in $c_{1/2}$ values further supports a D69K-induced reduction in fibril stability.

■ DISCUSSION

The results in Figure 1 show significant changes in the fluorescence properties of W26 on fibril formation by both WT and D69K apoC-II. The changes occur more rapidly for D69K fibrils, implying faster fibril formation, an effect we have previously attributed to the loss of an inhibitory effect of D69 on WT fibril formation.[16] A consequence of the D69K mutation is the loss of a charged pair (K30-D69) and the associated need to accommodate two lysine residues within the fibril core. While buried lysine residues have been observed in other protein systems,[33-35]
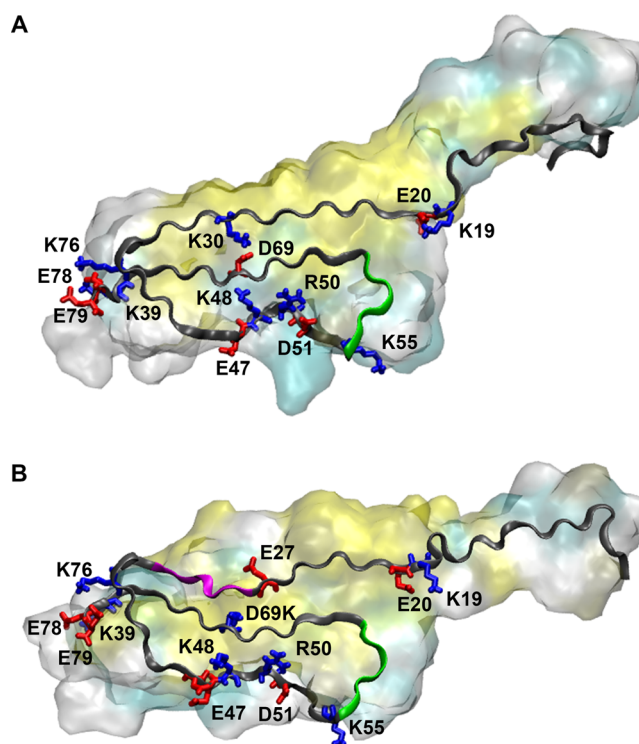
Figure 10. Persistent salt bridges (shown as licorice) in the (A) WT and (B) D69K fibril, superimposed over the vdW surface cloud representation of volume occupied by the D69K tetramer, colored on the basis of the predominant secondary structure (yellow for β strand, white for coil, and cyan for turn). Important regions discussed in the text are also highlighted. The region of reduced β-strand content in D69K (residues 29−34) is found opposite the mutation site and is colored magenta on the ribbon representation of the fibril model. Residues 57−62 are toward the N-terminus of the strand and are relatively distant from the mutation site in both WT and D69K fibrils (green).

there appear to be no precedents for buried charge residues within the cross-β core regions of amyloid fibrils. This feature may be peculiar to fibrils formed by members of the apolipoprotein family[1-7] for which their dual abilities to form both amphipathic α helices and cross-β structures impose constraints on the distribution of charged residues within the fibrils.

The results of our H/D exchange, X-ray diffraction, and MD studies show a remarkable overall degree of similarity between WT and D69K apoC-II fibrils, implying very similar fibril morphologies. Sedimentation velocity and electron microscopy studies confirm this conclusion.[16] Similar observations have also been reported for Aβ fibrils in which a series of mutant forms were found to influence fibril kinetics and dynamics but leave the general fibril structure unchanged.[36] However, while the overall
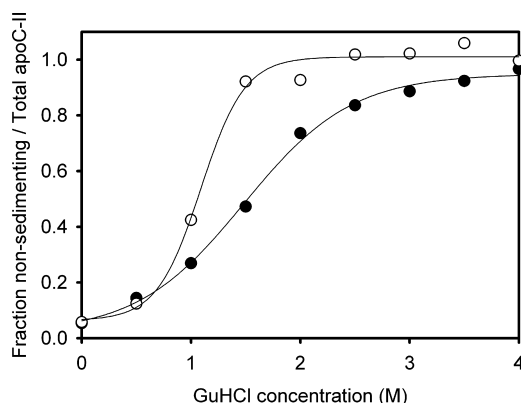
Figure 11. Analysis of fibril stabilities. Preformed WT (●) and D69K (○) apoC-II fibrils were incubated for 24 h at various GuHCl concentrations. The amount of apoC-II present in the supernatants following centrifugation at 100000 rpm (436000g) for 30 min was estimated by optical absorbance measurements at 280 nm. Data are presented as fractions relative to absorbances at 280 nm for uncentrifuged samples in 6 M GuHCl. The lines drawn through the data are best-fit lines using a four-parameter sigmoid function.

structure of apoC-II fibrils is maintained, there are significant changes at the detailed structural level. Most significant is the overall decrease in the level of H/D exchange protection for D69K apoC-II fibrils compared to WT fibrils, indicating more rapid H/D exchange for residues within the fibril core and lower fibril stability. This change in fibril stability is supported by the MD simulations that show a significant decrease in β-sheet structure content consistent with an increase in structural flexibility and solvent exposure, and by the GuHCl denaturation studies indicating less GuHCl is required for half-dissociation of D69K apoC-II fibrils than for that of WT. Another significant and perhaps related change is the increased distance between the β sheets revealed by the X-ray diffraction results and supported by the MD simulations. This structural change in D69K apoC-II fibrils is also accompanied by the formation of a stable E27-K69 salt bridge, an increase in the water content near the aromatic rings within the core region, and a reduction in the degree of in-register π-stacking formed by W26. These results indicate that while the loss of the K30-D69 charge pair does not prohibit fibril formation, the presence of two lysine residues within the core region significantly alters the stability and dynamics of fibrils.

It is of interest to compare these structural perturbations in the core region of D69K apoC-II fibrils and specifically the increased dynamics of W26 with the results of the acrylamide-induced fluorescence quenching studies. We propose two possible explanations to reconcile our observations that D69K apoC-II fibrils are less stable and more dynamic than WT fibrils while the level of acrylamide-induced fluorescence quenching of W26 is reduced. The presence of an additional lysine residue within this core region may inhibit the entry of acrylamide and reduce the extent of quenching. Alternatively, differences in the degree of in-register π-stacks formed by W26 in D69K apoC-II fibrils may affect the efficiency of acrylamide-induced fluorescence quenching.

The D69K mutation lies within the C-terminal β strand (residues 58−74) of apoC-II fibrils and a highly conserved α-helical lipoprotein lipase-activating domain.[15] The mutation has a significant effect on the calculated hydrophobic moment of the fragment of residues 58−74. The calculated values for the WT and D69K fragments are 3.9 and 3.5 kTÅ/e, respectively.[37] The decrease in the amphipathicity of this region for the D69K

fragment could exert a direct effect on the structure of the monomeric species that self-assemble into amyloid fibrils. D69K apoC-II forms fibrils more rapidly than WT apoC-II, suggesting that increased levels of transient α-helical structures in WT, compared to D69K apoC-II, reduce the relative rates of fibril formation. For both mature WT and D69K fibrils, fibril stability is facilitated by the formation of numerous salt bridges in the flexible connecting loops. This suggests that a major contributor of the increased stability of WT fibrils compared to that of D69K apoC-II fibrils is the ability to form a K30-D69 charge-pair interaction within the fibril core. This interaction is lost in the D69K apoC-II mutant but partly compensated by the formation of an alternate E27-K69 ion pair. These results highlight the important stabilizing effects of charge-pair interactions within the amyloid core of apoC-II fibrils that could account for the general ability of apolipoproteins to form both amphipathic α helices in the presence of lipid and cross-β fibrillar structures in the lipid-free state.

■ ASSOCIATED CONTENT

ⓢ Supporting Information

The Supporting Information is available free of charge on the ACS Publications website at DOI: 10.1021/acs.bio-chem.5b00535.

Supporting materials (PDF)

■ AUTHOR INFORMATION

Corresponding Author

*Department of Biochemistry and Molecular Biology, Bio21 Molecular Science and Biotechnology Institute, University of Melbourne, 30 Flemington Rd., Parkville, Victoria 3010, Australia. Telephone: 61-3-8344-2273. Fax: 61-3-9348-1421. E-mail: prg@unimelb.edu.au.

■ ABBREVIATIONS

apo, apolipoprotein; WT, wild type; d_6-DMSO, d_6-dimethyl sulfoxide; d_2-DCA, d_2-dichloroacetic acid; H/D, hydrogen/deuterium; HSQC, heteronuclear single-quantum coherence; XRD, X-ray fiber diffraction; MD, molecular dynamics; GuHCl, guanidine hydrochloride.

■ REFERENCES

(1) Sipe, J. D., and Cohen, A. S. (2000) Review: history of the amyloid fibril. *J. Struct. Biol. 130*, 88−98.

(2) Westermark, P., Mucchiano, G., Marthin, T., Johnson, K. H., and Sletten, K. (1995) Apolipoprotein A1-derived amyloid in human aortic atherosclerotic plaques. *Am. J. Pathol. 147*, 1186−1192.

(3) Higuchi, K., Kitagawa, K., Naiki, H., Hanada, K., Hosokawa, M., and Takeda, T. (1991) Polymorphism of apolipoprotein A-II (apoA-II) among inbred strains of mice. Relationship between the molecular type of apoA-II and mouse senile amyloidosis. *Biochem. J. 279* (Part 2), 427−433.

(4) Bergstrom, J., Murphy, C. L., Weiss, D. T., Solomon, A., Sletten, K., Hellman, U., and Westermark, P. (2004) Two different types of amyloid deposits–apolipoprotein A-IV and transthyretin–in a patient with systemic amyloidosis. *Lab. Invest. 84*, 981−988.

(5) Stewart, C. R., Haw, A., 3rd, Lopez, R., McDonald, T. O., Callaghan, J. M., McConville, M. J., Moore, K. J., Howlett, G. J., and O'Brien, K. D. (2007) Serum amyloid P colocalizes with apolipoproteins in human atheroma: functional implications. *J. Lipid Res. 48*, 2162−2171.

(6) Wisniewski, T., Lalowski, M., Golabek, A., Vogel, T., and Frangione, B. (1995) Is Alzheimer's disease an apolipoprotein E amyloidosis? *Lancet 345*, 956−958.

(7) O'Brien, K. D., Olin, K. L., Alpers, C. E., Chiu, W., Ferguson, M., Hudkins, K., Wight, T. N., and Chait, A. (1998) Comparison of apolipoprotein and proteoglycan deposits in human coronary atherosclerotic plaques: colocalization of biglycan with apolipoproteins. *Circulation 98*, 519−527.

(8) Corder, E. H., Saunders, A. M., Strittmatter, W. J., Schmechel, D. E., Gaskell, P. C., Small, G. W., Roses, A. D., Haines, J. L., and Pericak-Vance, M. A. (1993) Gene dose of apolipoprotein E type 4 allele and the risk of Alzheimer's disease in late onset families. *Science 261*, 921−923.

(9) Teoh, C. L., Griffin, M. D., and Howlett, G. J. (2011) Apolipoproteins and amyloid fibril formation in atherosclerosis. *Protein Cell 2*, 116−127.

(10) Li, W. H., Tanimura, M., Luo, C. C., Datta, S., and Chan, L. (1988) The apolipoprotein multigene family: biosynthesis, structure, structure-function relationships, and evolution. *J. Lipid Res. 29*, 245−271.

(11) Segrest, J. P., Garber, D. W., Brouillette, C. G., Harvey, S. C., and Anantharamaiah, G. M. (1994) The amphipathic alpha helix: a multifunctional structural motif in plasma apolipoproteins. *Adv. Protein Chem. 45*, 303−369.

(12) Hatters, D. M., and Howlett, G. J. (2002) The structural basis for amyloid formation by plasma apolipoproteins: a review. *Eur. Biophys. J. 31*, 2−8.

(13) Teoh, C. L., Pham, C. L., Todorova, N., Hung, A., Lincoln, C. N., Lees, E., Lam, Y. H., Binger, K. J., Thomson, N. H., Radford, S. E., Smith, T. A., Muller, S. A., Engel, A., Griffin, M. D., Yarovsky, I., Gooley, P. R., and Howlett, G. J. (2011) A Structural Model for Apolipoprotein C-II Amyloid Fibrils: Experimental Characterization and Molecular Dynamics Simulations. *J. Mol. Biol. 405*, 1246−1266.

(14) MacPhee, C. E., Howlett, G. J., Sawyer, W. H., and Clayton, A. H. (1999) Helix-helix association of a lipid-bound amphipathic alpha-helix derived from apolipoprotein C-II. *Biochemistry 38*, 10878−10884.

(15) Kinnunen, P. K., Jackson, R. L., Smith, L. C., Gotto, A. M., Jr., and Sparrow, J. T. (1977) Activation of lipoprotein lipase by native and synthetic fragments of human plasma apolipoprotein C-II. *Proc. Natl. Acad. Sci. U. S. A. 74*, 4848−4851.

(16) Mao, Y., Teoh, C. L., Yang, S., Zlatic, C. O., Rosenes, Z. K., Gooley, P. R., Howlett, G. J., and Griffin, M. D. (2015) Charge and Charge-Pair Mutations Alter the Rate of Assembly and Structural Properties of Apolipoprotein C-II Amyloid Fibrils. *Biochemistry 54*, 1421−1428.

(17) Cai, M., Huang, Y., Sakaguchi, K., Clore, G. M., Gronenborn, A. M., and Craigie, R. (1998) An efficient and cost-effective isotope labeling protocol for proteins expressed in Escherichia coli. *J. Biomol. NMR 11*, 97−102.

(18) Marley, J., Lu, M., and Bracken, C. (2001) A method for efficient isotopic labeling of recombinant proteins. *J. Biomol. NMR 20*, 71−75.

(19) Hoshino, M., Katou, H., Hagihara, Y., Hasegawa, K., Naiki, H., and Goto, Y. (2002) Mapping the core of the beta(2)-microglobulin amyloid fibril by H/D exchange. *Nat. Struct. Biol. 9*, 332−336.

(20) Zhang, Y. Z., Paterson, Y., and Roder, H. (1995) Rapid Amide Proton-Exchange Rates in Peptides and Proteins Measured by Solvent Quenching and 2-Dimensional Nmr. *Protein Sci. 4*, 804−814.

(21) Yamaguchi, K. I., Katou, H., Hoshino, M., Hasegawa, K., Naiki, H., and Goto, Y. (2004) Core and heterogeneity of beta(2)-microglobulin amyloid fibrils as revealed by H/D exchange. *J. Mol. Biol. 338*, 559−571.

(22) Delaglio, F., Grzesiek, S., Vuister, G. W., Zhu, G., Pfeifer, J., and Bax, A. (1995) NMRPipe: a multidimensional spectral processing system based on UNIX pipes. *J. Biomol. NMR 6*, 277−293.

(23) Johnson, B. A., and Blevins, R. A. (1994) NMR View: A computer program for the visualization and analysis of NMR data. *J. Biomol. NMR 4*, 603−614.

(24) Serpell, L. C., Fraser, P. E., and Sunde, M. (1999) X-ray fiber diffraction of amyloid fibrils. *Methods Enzymol. 309*, 526−536.

(25) Sumner Makin, O., Sikorski, P., and Serpell, L. C. (2007) CLEARER: a new tool for the analysis of X-ray fibre diffraction patterns and diffraction simulation from atomic structural models. *J. Appl. Crystallogr. 40*, 966−972.

(26) Bussi, G., Donadio, D., and Parrinello, M. (2007) Canonical sampling through velocity rescaling. *J. Chem. Phys. 126*, 014101.

(27) Parrinello, M., and Rahman, A. (1981) Polymorphic Transitions in Single-Crystals - a New Molecular-Dynamics Method. *J. Appl. Phys. 52*, 7182−7190.

(28) Hess, B., Bekker, H., Berendsen, H. J. C., and Fraaije, J. G. E. M. (1997) LINCS: A linear constraint solver for molecular simulations. *J. Comput. Chem. 18*, 1463−1472.

(29) Humphrey, W., Dalke, A., and Schulten, K. (1996) VMD: Visual molecular dynamics. *J. Mol. Graphics 14*, 33−38.

(30) Baldwin, A. J., Knowles, T. P. J., Tartaglia, G. G., Fitzpatrick, A. W., Devlin, G. L., Shammas, S. L., Waudby, C. A., Mossuto, M. F., Meehan, S., Gras, S. L., Christodoulou, J., Anthony-Cahill, S. J., Barker, P. D., Vendruscolo, M., and Dobson, C. M. (2011) Metastability of Native Proteins and the Phenomenon of Amyloid Formation. *J. Am. Chem. Soc. 133*, 14160−14163.

(31) Wilson, L. M., Mok, Y. F., Binger, K. J., Griffin, M. D., Mertens, H. D., Lin, F., Wade, J. D., Gooley, P. R., and Howlett, G. J. (2007) A structural core within apolipoprotein C-II amyloid fibrils identified using hydrogen exchange and proteolysis. *J. Mol. Biol. 366*, 1639−1651.

(32) Sunde, M., Serpell, L. C., Bartlam, M., Fraser, P. E., Pepys, M. B., and Blake, C. C. (1997) Common core structure of amyloid fibrils by synchrotron X-ray diffraction. *J. Mol. Biol. 273*, 729−739.

(33) Isom, D. G., Cannon, B. R., Castaneda, C. A., Robinson, A., and Garcia-Moreno, B. (2008) High tolerance for ionizable residues in the hydrophobic interior of proteins. *Proc. Natl. Acad. Sci. U. S. A. 105*, 17784−17788.

(34) Takayama, Y., Castaneda, C. A., Chimenti, M., Garcia-Moreno, B., and Iwahara, J. (2008) Direct evidence for deprotonation of a lysine side chain buried in the hydrophobic core of a protein. *J. Am. Chem. Soc. 130*, 6714−6715.

(35) Isom, D. G., Castaneda, C. A., Cannon, B. R., and Garcia-Moreno, B. (2011) Large shifts in pKa values of lysine residues buried inside a protein. *Proc. Natl. Acad. Sci. U. S. A. 108*, 5260−5265.

(36) Adler, J., Scheidt, H. A., Kruger, M., Thomas, L., and Huster, D. (2014) Local interactions influence the fibrillation kinetics, structure and dynamics of A beta(1−40) but leave the general fibril structure unchanged. *Phys. Chem. Chem. Phys. 16*, 7461−7471.

(37) Reisser, S., Strandberg, E., Steinbrecher, T., and Ulrich, A. S. (2014) 3D Hydrophobic Moment Vectors as a Tool to Characterize the Surface Polarity of Amphiphilic Peptides. *Biophys. J. 106*, 2385−2394.